# Spiral-Mediated Growth Can Lead to Crystals of Higher Purity

**ARTICLE** *in* CRYSTAL GROWTH & DESIGN · MAY 2012

Impact Factor: 4.89 · DOI: 10.1021/cg300024f



**3 AUTHORS:**

Mike Sleutel
Vrije Universiteit Brussel
**30** PUBLICATIONS **205** CITATIONS
SEE PROFILE

Gen Sazaki
Hokkaido University
**166** PUBLICATIONS **2,449** CITATIONS
SEE PROFILE

Alexander E.S. Van Driessche
Vrije Universiteit Brussel
**44** PUBLICATIONS **348** CITATIONS
SEE PROFILE

CRYSTAL GROWTH & DESIGN

Article

pubs.acs.org/crystal

# Spiral-Mediated Growth Can Lead to Crystals of Higher Purity

Mike Sleutel,[†] Gen Sazaki,[‡] and Alexander E. S. Van Driessche*[,§]

[†]Structural Biology Brussels, Flanders Interuniversity Institute for Biotechnology (VIB), Vrije Universiteit Brussel, Pleinlaan 2, 1050, Elsene, Belgium

[‡]The Institute of Low Temperature Science, Hokkaido University, N19-W8, Sapporo 060-0819, Japan

[§]Laboratorio de Estudios Crystalograficos, IACT, CSIC − U. Granada, P.T. Ciencias de la Salud, Avenida del conocimiento s/n, 18100 Armilla (Granada), Spain

**ABSTRACT:** The morphology and step kinetics of 2D islands and spiral hillocks of lysozyme crystals growing from purified and contaminated solutions were determined and compared. It was found that the morphology and step dynamics of spiral hillocks of lysozyme crystals are less affected by the presence of impurities in the growth solution as compared to steps generated by 2D nucleation. These observations could be satisfactorily explained considering the terrace exposure time of spiral hillocks ($\tau_{sp}$) and 2D islands ($\tau_{2D}$) and the characteristic impurity adsorption time ($\tau_i$). For lysozyme, overlapping time scales of terrace exposure and impurity adsorption exist and $\tau_i \approx \tau_{sp} < \tau_{2D}$. Hence, when crystal growth is dominated by spiral hillocks, less impurities are adsorbed onto the crystal surface and a more pure crystal lattice is formed. Although spiral hillocks reduce the effect of impurities, they do play a significant role in the mechanism of step bunching.

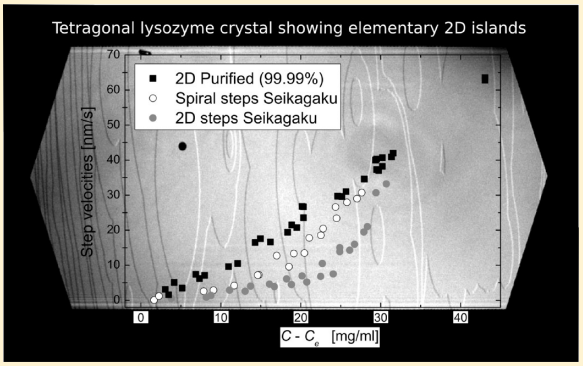


## INTRODUCTION

The predominant application of protein crystals is in the field of structural biology, where X-ray and neutron diffraction are used to resolve their 3D structure. When crystals are used for this purpose, the diffraction quality is highly decisive for the level of resolution obtainable in the final 3D model. One of the key factors affecting the diffraction quality of a crystal is the solution purity from which the crystal was grown.[1−4] This is mainly the result of a reduced internal order (e.g., lattice defects) of crystals that incorporated impurities during their growth. The influence of impurities in protein crystallization is highly relevant because target samples are consistently contaminated by large quantities (≥5%) of protein material.[5] Although the influence of impurities on the crystallization process already starts at the nucleation stage, inducing for example strain fields in the core of the crystals,[6] these effects are not addressed here. In this work, we focused solely on impurity effects restricted to growth.[7]

The art of high-quality protein crystallization is still, in essence, based on a trial and error methodology. To improve the success of rate of growing high-quality protein crystals, it is paramount to obtain a more profound understanding of the relationship between growth mechanisms and impurity adsorption on the crystal surface and posterior incorporation of these impurities in the crystal lattice. Spiral growth and two-dimensional (2D) nucleation have been identified as the main growth mechanisms for protein crystals growing from solution.[8−10] In the literature, we can find multiple studies on the effect of impurities on spiral hillocks[11,12] and 2D islands.[11,13,14] Yet, up to now, no direct comparison between the influence of impurities on growth steps emanating from a spiral dislocation and 2D islands under otherwise identical conditions has been performed. In principle, there should be no difference in step structure for spiral hillocks or 2D islands; thus the mechanism and rate of impurity incorporation should be identical for both growth mechanisms. However, terrace exposure times ($\tau$) may vary between spiral and 2D nucleation growth, and with it, the amount of impurity incorporated by the growing crystal. Therefore, in this work, we investigated the influence of protein impurities on the morphology and growth kinetics of spiral hillocks and 2D islands on the {110} face of lysozyme crystals for a broad supersaturation range. Tetragonal crystals of lysozyme are excellent model systems for this purpose because they can either grow by the 2D nucleation mechanism or grow by the spiral dislocation mechanism over a wide supersaturation range.[15−17]

## MATERIALS AND METHODS

**In Situ Observation of Step Dynamics on a Protein Crystal Surface.** Laser confocal differential interference contrast microscopy (LCM-DIM)[18] was used for in situ observation of {110} faces of growing lysozyme crystals. This setup is built around a confocal system (FV300, Olympus) attached to an inverted optical microscope (IX70, Olympus) with a 20× objective lens (LUCplan FLN 20×, Olympus) and equipped with a Nomarski prism introduced into the optical path and a partially coherent superluminiscent diode (Amonics Ltd., model

Received: January 8, 2012
Revised: February 24, 2012

   dx.doi.org/10.1021/cg300024f | Cryst. Growth Des. XXXX, XXX, XXX−XXX

ASLD68-050-B-FA: 680 nm) to eliminate diffraction noise. More details about this experimental setup can be found in previous works.[19−21]

The observation cell (1 × 10 × 15 mm$^3$, volume = 150 $\mu$L) used in this work was made out of two sandwiched glass plates of 0.17 mm thickness separated by 1 mm thick polystyrene spacers glued by silicone adhesive to one of the glass plates. After the polymerization of the adhesive, the cell was carefully washed by ultrasonic cleaning in pure (Milli-Q) water. Previously grown seed crystals of lysozyme (≥30 $\mu$m in height) were transferred to the observation cell with the {110} faces parallel to the bottom glass plate. Step movement was observed at the free (upper) solution−crystal interface. The observation cell was mounted inside a copper sample stage, which completely surrounds the observation cell, except for the observation area (Ø7 mm) at the bottom side. To precisely control the temperature of the sample stage, a curve-matched thermistor, two peltiers elements, and a PR-59 (Supercool ) temperature controller PC-interfaced through a serial connection by means of a Labview driver developed at our laboratory were used. Thermal silicon grease was employed to minimize thermal contact resistance. The precision of the temperature control (±0.1 °C) in the studied temperature range (17−27 °C) was only limited by the sensor accuracy.[20]

**Protein Solutions and Seed Crystals.** Prior to use, all lysozyme solutions were two times dialyzed against a 50 mM sodium acetate pH 4.5 buffer using a dialysis membrane with molecular weight cut off of 3500. Tetragonal seed crystals of lysozyme were grown at 20.0 ± 0.1 °C from a solution containing 60 mg/mL commercial grade lysozyme (≥98.0%, Seikagaku), 25 mg/mL NaCl, and 50 mM sodium acetate pH 4.5 buffer. After seed crystals were transferred to the observation cell, the solution was replaced with a solution of desired concentration. Two types of solutions were used for the in situ observation experiments: (1) highly purified lysozyme solution (99.99%, Maruwa Food Industries, Inc.) and (2) Seikagaku lysozyme (98.5%). The purity level of the Maruwa sample (99.99%) was verified by sodium dodecylsulfate polyacrylamide gel electrophoresis (SDS-PAGE) with enhanced silver staining (detection limit ≤0.01%), and no traces of impurities could be found. Impurity content of the Seikagaku sample (98.5%) was also confirmed by SDS-PAGE: The Seikagaku sample contained ∼0.5% dimer and ∼1.0% 18 kDa, as reported by Thomas and co-workers.[22] Before and after each experimental run, the protein concentration was determined at 280 nm with $\varepsilon_{280}$ = 2.64 mL/mg.cm[23] using a Cary 1E (Varian, Palo alto, CA) two-beam spectrophotometer from which no significant difference in concentration could be discerned.

Orthorhombic glucose isomerase crystals from Streptomyces rubiginosus (Macrocrystal Oy) were crystallized and imaged as described in ref 16. Glucose isomerase batches obtained from Macrocrystal Oy are of high purity level; however, they can contain small but varying degrees of impurity content. The nonpure data for glucose isomerase were obtained using a single batch with an unusually high impurity level (details to be published).

## RESULTS

**Impurities Lead to Step Rounding and Nonlinear Growth Rate Dependencies.** A series of in situ LCM-DIM images of a {110} face growing by the spiral dislocation mechanism and another {110} face growing by the 2D nucleation mechanism are shown in Figure 1a−d. Spiral hillocks and 2D islands that formed in a 99.99% pure lysozyme solution on {110} faces are lens-shaped with sharp tips (Figure 1 a−d). This strongly anisotropic step shape is the result of different packing of molecules in the (110) and (001) directions[24] and the consequent kinetic anisotropy in the step advancement in both directions. In Figure 1e, step velocities measured on the {110} faces for spiral hillocks and 2D islands are compared. No different supersaturation dependency is found for these two step sources. Nevertheless, a distinct difference in step velocity for each crystallographic direction is found. This demonstrates, as mentioned before, that the characteristic step shape results from an intrinsic anisotropy in the step velocities, with [110] the fast direction, *a*, and [001] the slow direction, *b*. The ratio of fast to slow directions of 2D islands and spiral hillocks on the {110} face is $a/b \approx 6$ and does not change with supersaturation (Figure 1e). Step velocities, in both crystallographic directions, show an almost linear dependency on absolute supersaturation.

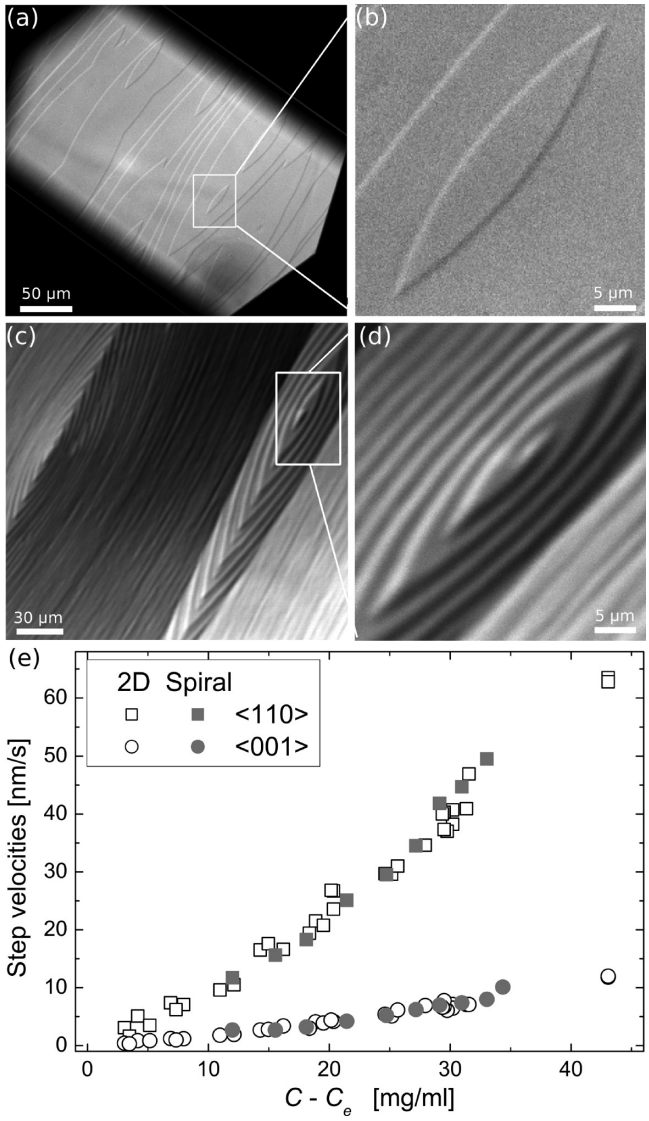


**Figure 1.** Step morphology of spiral hillocks (a) and 2D islands (b) on {110} faces of tetragonal lysozyme crystals growing from a purified lysozyme solution. Anisotropy of a 2D island (c) and spiral hillock (d) formed from purified lysozyme solutions. The ratio of the short and long axis of 2D islands and spiral hillocks $a/b$ is approximately 6. (e) Supersaturation dependencies of tangential step growth rates in different crystallographic directions of spiral hillocks and 2D islands on {110} faces of tetragonal lysozyme crystals.

Figure 2a−d shows in situ LCM-DIM images of a spiral hillock and 2D islands on {110} faces of lysozyme crystals growing from contaminated solutions (∼98.5%, Seikagaku). In the low to middle supersaturation range ($C - C_e$ = 0−25 mg/mL), a significant difference in step morphology is observed as compared to steps formed in purified solutions. Both spiral hillocks and 2D islands formed in the ∼98.5% pure lysozyme solution exhibit rounded tips with certain roughness caused by


dx.doi.org/10.1021/cg300024f | Cryst. Growth Des. XXXX, XXX, XXX−XXX

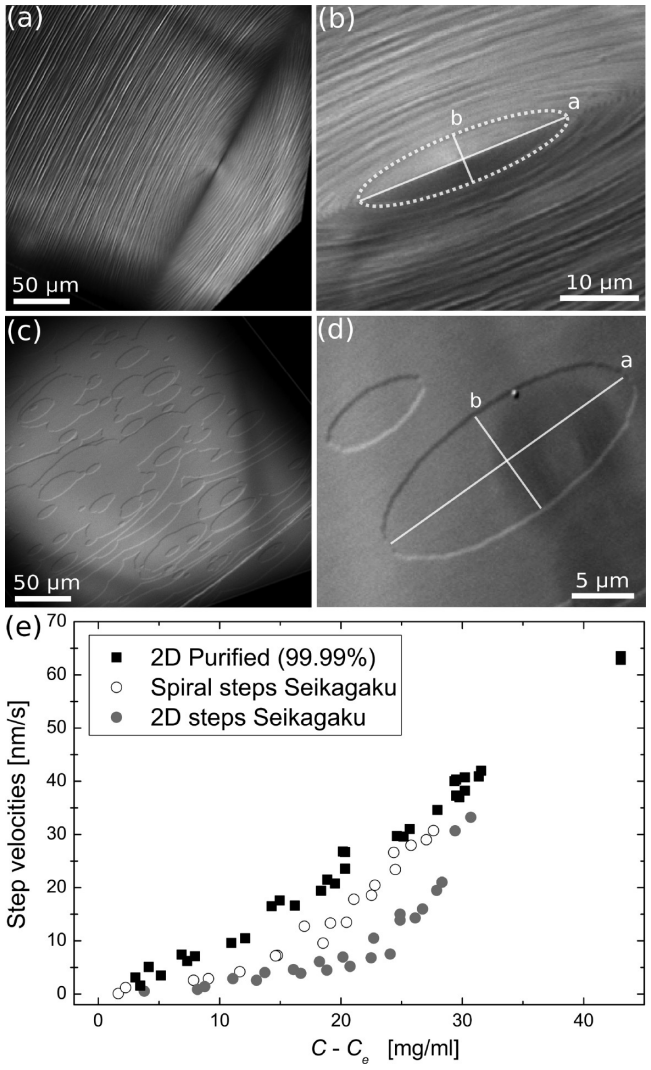


**Figure 2.** Step morphology of spiral hillocks (a) and 2D islands (b) on {110} faces of tetragonal lysozyme crystals growing from a Seikagaku lysozyme solution containing covalently bounded lysozyme dimers and 18 kDa polypeptides. Detail of the morphology of 2D islands (c) and spiral hillocks (d) growing from Seikagaku lysozyme. The ratio of the short and long axis, $a/b$, of 2D islands is approximately 3 and approximately 4 for spiral hillocks. (e) Step velocities in the ⟨110⟩ directions of 2D islands and spiral hillocks growing from Purified and Seikagaku lysozyme as a function of supersaturation.

step pinning due to impurities adsorbed on the surface.[24,25] In the case of 2D islands, a ratio of $a/b \approx 3$ is found, while for spiral hillocks a ratio of $a/b \approx 5$ is found (Figure 2b and d). The results of step velocity measurements of 2D islands and spiral hillocks growing from contaminated solutions (~98.5%, Seikagaku) are presented in Figure 2e. A clear difference in supersaturation dependencies for step velocities of spiral hillocks and 2D islands is found for the ⟨110⟩ direction. This different dependency of step velocity on supersaturation was also observed for the ⟨001⟩ direction (data not shown). For the second model protein system, glucose isomerase, a series of experiments were conducted comparing morphologies of 2D islands and spiral hillocks grown from uncontaminated solutions and contaminated solutions. In Figure 3, examples are shown of the step morphology on the {011} face of glucose isomerase. Just as in the case of lysozyme, when impurities are present the corners of steps become rounded, indicating that mainly the fast growing directions are affected by the presence of impurities. We do not observe a strong difference in step shape between spiral and 2D steps for this model system. These qualitative results suggest that impurities are incorporated in similar amounts by both layer mechanisms; however, further quantitative evidence is needed to elucidate matters further.

**Terrace Exposure Time Is Layer Generation Dependent.** On the basis of single molecule fluorescence microscopy experiments,[25] it is known that the main impurities (lysozyme dimer, 18 kDa polypeptide) present in Seikagaku lysozyme solutions adsorb randomly on the terraces leading to pinning of the steps. For these impurities to reach appreciable surface concentrations, the characteristic time for adsorption $\tau_{imp}$ needs to be equal to or smaller than the average exposure time of a terrace $\tau_{terr}$. Note that for impurities that preferentially bind to kink sites (kink blocking mechanism), the kink exposure time $\tau_{kink}$ becomes the relevant parameter; given the nature of the impurities used in this study, in our further analysis we do not take $\tau_{kink}$ into consideration. Thus, if impurity effects want to be estimated, the terrace exposure time needs to be determined. This can be calculated analytically for spiral and 2D-mediated growth using the following expressions:[26]

$$\tau_{spiral} = \frac{\lambda}{v_{step}} = \frac{19\kappa a^2}{kT\ln(C/C_e)\beta_{step}\Omega(C - C_e)} \quad (1)$$

$$\tau_{2D} = \frac{h}{R} = \frac{h}{h[\pi v_{step}^2 J]^{1/3}} = \left[\pi(\Omega\beta(C - C_e))^2\omega^*\Gamma Z\exp\left(-\frac{\pi\kappa^2 s}{k^2T^2\ln(C/C_e)}\right)\right]^{-1/3} \quad (2)$$

with eq 1 based on an isotropic spiral and eq 2 assuming multilayer 2D growth, which is a valid assumption given that true layer-by-layer growth is quasi never achieved in lysozyme and glucose isomerase crystal growth.[17] Figure 4 shows the dependency of the terrace exposure time $\tau$ for the spiral and 2D case as a function of $\ln(C/C_e)$ for lysozyme and glucose isomerase. These plots have been obtained by inserting the experimentally obtained values of the fundamental growth parameters (see Table 1) into eqs 1 and 2. $\tau$ decreases strongly with increasing supersaturation, asymptotically approaching zero for high $\ln(C/C_e)$ values. Typically, $\tau_{spiral}$ values for high $\ln(C/C_e)$ cannot be obtained experimentally because step generation will be dominated by 2D nucleation and any spirals present on the surface will be overgrown. Figure 4 shows that the terrace exposure times of spirals are consistently smaller than those of 2D terraces throughout the entire supersaturation window. Although this general trend applies to both proteins, we do observe a quantitative difference: the relative gap between spiral and 2D appears much more pronounced for the case of lysozyme, which can be attributed to the lower step kinetic coefficient and the higher step edge free energy as compared to glucose isomerase.

The similarity in step structure between 2D and spiral steps for impure glucose isomerase (Figure 3) suggests that the kinetics of impurity adsorption are faster than layer generation for either mechanism. We do note that only conditions relatively close to equilibrium and therefore with long terrace exposure times were tested in this study. Experiments in higher supersaturation regimes could reveal a crossover point in


dx.doi.org/10.1021/cg300024f | Cryst. Growth Des. XXXX, XXX, XXX−XXX

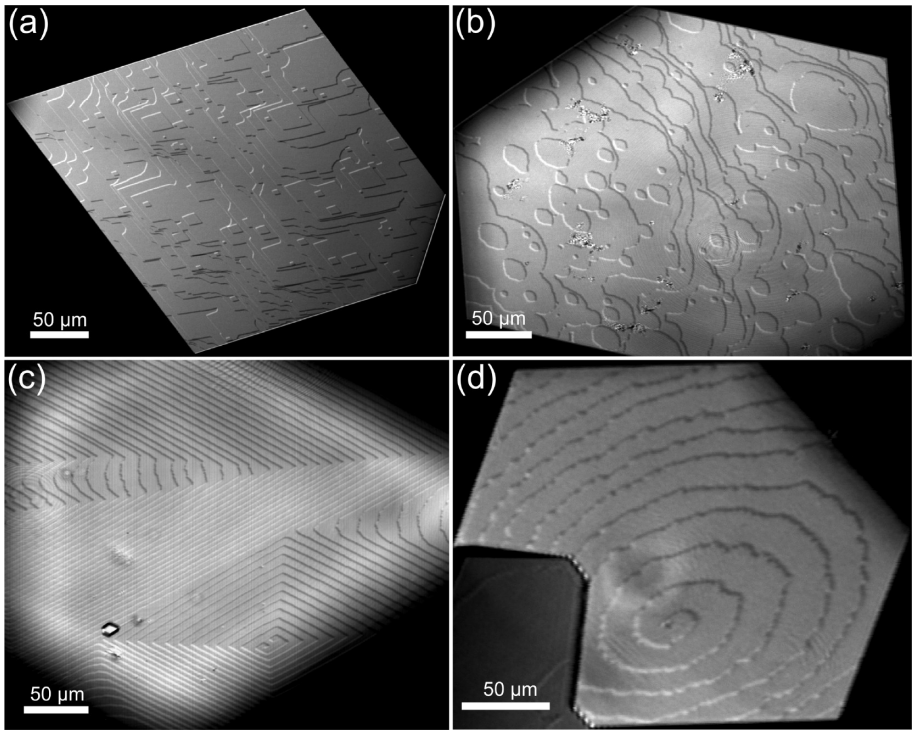


**Figure 3.** Step morphology of spiral hillocks and 2D islands on {011} faces of orthorhombic glucose isomerase crystals growing from pure (a,c) or impure solutions (b,d).

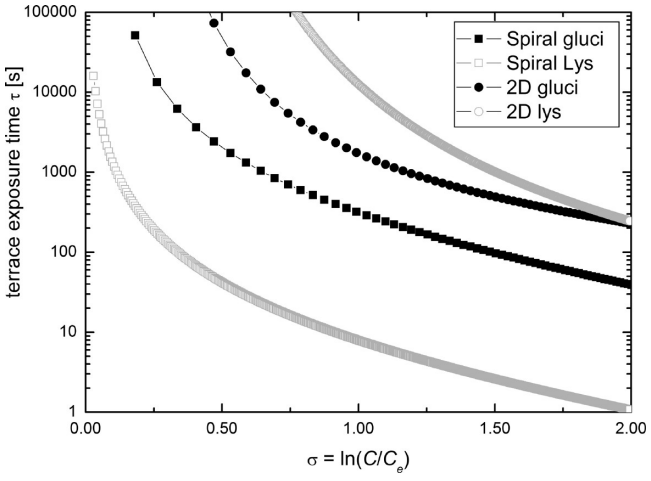


**Figure 4.** Terrace exposure time $t$ as a function of driving force $\ln(C/C_e)$ for spiral and 2D-mediated growth calculated from eqs 1 and 2 for lysozyme and glucose isomerase.

growth regimes characterized by differences in step structure and kinetics for both layer generation mechanisms in impure conditions.

**Impurities Lead to Increased Step Bunching.** Although the LCM-DIM technique does not allow one to determine quantitatively the surface topography, relative height differences can be easily differentiated due to proportionality between step height and contrast.[15] During this work, we frequently observed that steps on spiral hillocks tend to coalescence into macrosteps. When 2D nucleation was the dominant growth mechanism, only the nucleation of multilayer islands was observed as a source of bunched steps in the studied supersaturation range. The origin of multilayer islands is not related to the mechanism of step bunching and is discussed in a

**Table 1. Experimental Parameters Used in the Calculation of the Plots Shown in Figure 4**

| | lysozyme[a] | glucose isomerase[b] |
|---|---|---|
| $T$ (K) | 293 | 293 |
| $\kappa_{HON}$ (J/m) | $3.5 \times 10^{-12}$ | $6.0 \times 10^{-13}$ |
| $a$ (m) | $2.8 \times 10^{-9}$ | $9.5 \times 10^{-9}$ |
| $\Omega$ ($m^3$) | $30 \times 10^{-27}$ | $4.99 \times 10^{-25}$ |
| $\beta_{step}$ (m/s) | $6.1 \times 10^{-7s}$ | $3.65 \times 10^{-6}$ |
| $C_e$ (mg/mL) | 13.6 | 0.1 |
| $\omega^*\Gamma Z$ ($m^2$/s) | $6.20 \times 10^{10}$ | $5.837 \times 10^{10}$ |
| $s$ ($m^2$) | $7.84 \times 10^{-18}$ | $9.7 \times 10^{-17}$ |

[a]Reference 15 and references therein. [b]Reference 16 and references therein.

previous work.[15] In Figure 5, typical LCM-DIM images of spiral hillocks (grown at constant supersaturation) with bunched steps on the {110} face are shown. The crystals in images a and b were grown from Seikagaku lysozyme, and the crystals in images c–e were grown from highly purified lysozyme solution. Step bunching was not observed close to the spiral dislocation outcrop, but always started at a certain distance from the spiral hillock center (see white and black lines in Figure 5). More importantly, when spiral hillocks grown from highly purified lysozyme are compared to those grown from Seikagaku lysozyme, it becomes evident that step bunching is much more pronounced for crystal growth from solutions containing impurities. No step bunching is observed in the ⟨110⟩ directions for crystals growing from purified solution (Figure 5c,d), while step bunching is observed in the ⟨001⟩ direction far from the dislocation outcrop (Figure 5c,d). On the other hand, for crystals grown in the presence of impurities, step bunching starts in both directions relatively close to the spiral center (Figure 5a,b).


dx.doi.org/10.1021/cg300024f | Cryst. Growth Des. XXXX, XXX, XXX–XXX

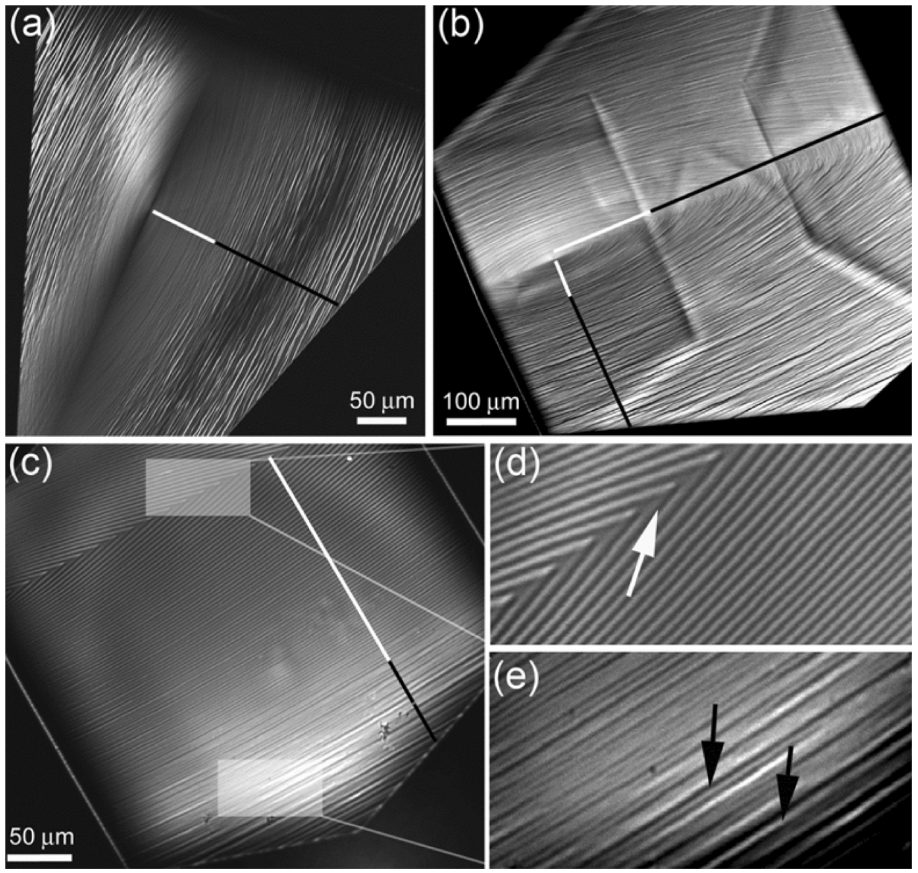


**Figure 5.** Step bunching observed by LCM-DIM on spiral hillocks. (a,b) Hillocks formed in commercial lysozyme. (c) A hillock formed in purified lysozyme showing close-ups of (d) the central area of the spiral and (e) edge of the crystal. White arrows and white lines indicate monolayer steps. Black arrows and black lines indicate bunched steps. Experimental conditions, supersaturation ($C - C_e$ = 24.4 mg/mL) and temperature (22.0 °C), were kept constant for several days.

## DISCUSSION

**Shorter Terrace Exposure Times Lead to Reduced Impurity Uptake.** Figure 1 shows that for purified lysozyme solution, step morphology and step velocity of spiral hillocks and 2D islands have the same dependency on supersaturation. This indicates, as expected, that step advancement and attachment kinetics of molecules to the surface do not depend on the step source. The interstep distance of steps originating from spiral hillocks is in the range of 1 $\mu$m to tens of nanometers, depending on the supersaturation and the crystallographic orientation. On the other hand, the interstep distance of monolayer 2D islands can easily reach several tens of micrometers for low supersaturations. Even so, all steps velocities show the same dependency on supersaturation (Figure 1). Thus, for the studied supersaturation range, steps do not interact, indicating that there is no significant overlap of (bulk and/or surface) diffusion fields surrounding the steps of spiral hillocks.

In the case of contaminated solutions (Figure 2), the advancement of steps originating from 2D islands and spiral hillocks displays a distinct behavior. From the observed surface morphologies and step velocities, it can be inferred that steps of spiral hillocks on the {110} face of lysozyme are less affected by impurities as compared to 2D islands. In the case of glucose isomerase, no significant differences are detected. Because no intrinsic differences exist between step dynamics originating from spiral dislocations or 2D islands, the reduced impurity effect of spiral hillocks can only be understood in terms of a reduced impurity adsorption on the crystal surface. Assuming a kinetic (i.e., time-dependent) mechanism for impurity adsorption on the crystal surface (i.e., noninstantaneous binding), it is clear that for overlapping time scales of terrace exposure and impurity adsorption, surface concentrations of impurities will not reach equilibrium values.[27] Because of this difference in exposure times for both growth mechanisms, terraces on spiral hillocks will be relatively devoid of impurities as compared to areas where steps are generated by 2D nucleation. This is strongly corroborated by the kinetic data of lysozyme shown in Figure 2e where the stronger deceleration of step advancement for 2D steps is demonstrated. Most likely, this is a consequence of the smaller interstep distances found on spiral hillocks ($\geq$10 $\mu$m) as compared to typical interstep distances of 2D islands ($\geq$10 $\mu$m) at identical supersaturation levels, which eventually leads to lower terrace exposure times (Figure 4a). Taking into account that the two main impurities present in Seikagaku lysozyme, dimer and 18 kDa, randomly adsorb on terraces, a reduction in the terrace exposure time should lead to a decreased amount of impurities adsorbed on the terraces. This then translates into reduced step pinning and explains the increased step velocity and the step morphology observed for spiral hillocks.

To confirm this hypothesis, we tried to quantify the diminution in adsorption impurity molecules due to a reduction of the terrace exposure time of spiral hillocks compared to 2D islands. To do so, we considered a general impurity model, based on a step pinning mechanism, proposed by van der


dx.doi.org/10.1021/cg300024f | Cryst. Growth Des. XXXX, XXX, XXX−XXX

Eerden.[28] This model (eq 3), similar to the Cabrera–Vermilyea model (eq 5), predicts a reduction of the step velocity by a factor proportional to the density of impurities on the surface and the critical step curvature:

$$v_{step}(\Gamma_i) = v_{step}(\Gamma_i = 0)\left(1 - \frac{4\Gamma_i}{(K^*)^2}\right) \quad (3)$$

Here, $\Gamma_i$ is the surface concentration of impurities (number of impurity molecules per unit area), and $K^* = \sigma/d_0$ is the critical curvature for which steps stop advancing due to stress accumulation. Here, $\sigma = (C/C_e - 1)$ is the relative supersaturation, and $d_0$ is the edge capillary length and depends mainly on the step stiffness, an intrinsic constant of the step, that we consider to be invariable with impurity concentration. This assumption is based on the invariability of the apparent step stiffness as a function supersaturation for pure and impure growth conditions extracted from 2D nucleation rate determinations on lysozyme.[15] Rearranging eq 3 gives

$$\frac{v_{step}(\Gamma_i = 0)}{v_{step}(\Gamma_i = 0) - v_{step}(\Gamma_i)} = \frac{1}{4d_0^2\Gamma_i}\sigma^2 \quad (4)$$

reaching limiting values of ∞ and 1 for the pure case and maximal impurity effect, respectively. The slopes of this plot are inversely related to surface impurity concentration. Figure 6 shows that for identical supersaturation and impurity content, steps generated by 2D islands advance slower than steps emanating from a spiral dislocation; that is, the impurity effect is more pronounced in the 2D case. This is reflected back in the slope and nonlinearity of the plot. In the low supersaturation range, the slope of the spiral plot is consistently higher than that for the 2D data, indicating that the impurity surface concentration is lower on the terraces between the spiral steps. The slopes increase monotonically as a function of supersaturation for both cases (although more obvious in the 2D case); that is, the impurity surface concentration decreases as the supersaturation is increased (for constant impurity surface concentration, a linear plot would be obtained). We correlate this to the reduction in terrace exposure time at higher driving forces. From these data, we conclude that the smaller interstep distance of spiral hillocks has an "impurity blocking effect" reducing the concentration of impurity molecules at the crystal surface. At higher supersaturation, the interstep distance of a surface growing by 2D nucleation becomes considerably smaller and the impurity concentration at the crystal surface is also significantly reduced (Figure 6), which is demonstrated by the steep increase in slope for 2D islands at $\sigma \geq 3.5$. From the data presented in Figure 6, we conclude that the surface impurity concentration decreases monotonically with increasing supersaturation. This $\sigma$ dependence (and by extension $\tau$ dependence) of $\Gamma_i$ therefore needs to be explicitly accounted for in the models that predict step kinetics in impure conditions. Indeed, Weaver and co-workers derived such a time-dependent impurity model that is based on an expression for step velocity with step pinning that explicitly takes into account a dead zone supersaturation $\sigma_d$.[27]

We do not observe a clear dead zone for lysozyme, nor do we obtain an exponential dependence at high $\sigma$ as assumed in their base-model.[29] We therefore develop two similar models based on eq 3 and the Cabrera–Vermilyea model:

$$v_{step}(\Gamma_i) = v_{step}(\Gamma_i = 0)(1 - 2r_c(n_{max}\theta)^{1/2})^{1/2} \quad (5)$$

where $r_c$ is the critical radius and $\theta$ is the impurity surface coverage. Assuming Langmuir adsorption (Figure 7a) for the binding of impurities to the crystal surface, the change in impurity surface coverage becomes $d\theta/dt = C_i k_A(1 - \theta) - k_D\theta$

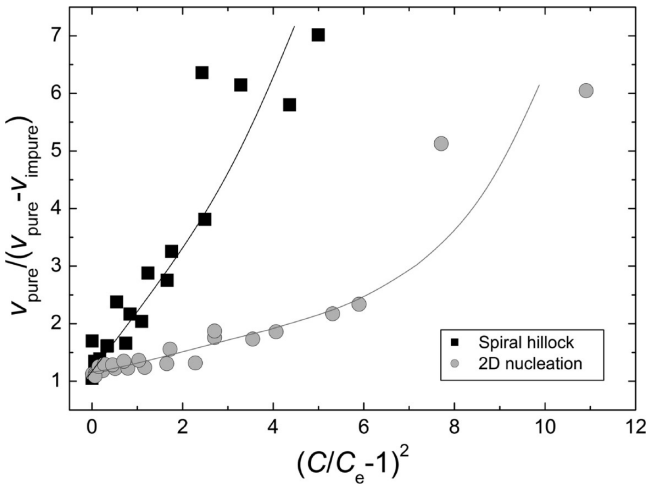


**Figure 6.** Plot of the inverse step deceleration as a function of squared supersaturation (eq 4) for the case of lysozyme. The slope of the plot is inversely proportional to the concentration of surface adsorbed impurities. Lines are guides for the eye.

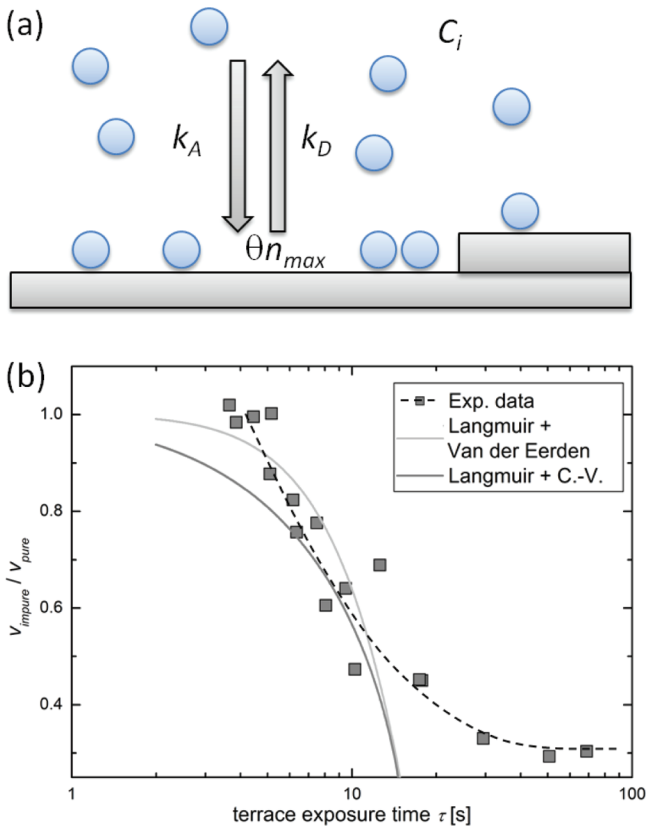


**Figure 7.** (a) Schematic representation of impurity adsorption onto the liquid/crystal interface (for details on the symbols, see text). (b) Reduction in step velocity $v_{impure}/v_{pure}$ as a function of terrace exposure time: experimental data (■ with dashed line as guide for the eye) and fits (full lines).


dx.doi.org/10.1021/cg300024f | Cryst. Growth Des. XXXX, XXX, XXX–XXX

with $k_A$ and $k_D$ the rate constants for adsorption and desorption and $C_i$ the bulk impurity concentration. Solving for $\theta$ yields[26]

$$\theta(t) = \theta_e(1 - e^{-\tau/\tau_i}) \quad \text{with} \quad \theta_e = \frac{C_i k_A}{C_i k_A + k_D} \quad \text{and} \quad \tau_i = (C_i k_A + k_D)^{-1} \tag{6}$$

with $\theta_e$ the equilibrium impurity surface coverage and $\tau_i$ the characteristic time for impurity binding. Inserting eq 6 into either expression for the step velocity in the presence of terrace adsorbed impurities and realizing that $\Gamma_i = n_{max}\theta(t)$ (with $n_{max}$ as the number of impurity adsorption sites), the dependence for the impurity effect on $\tau$ is obtained, respectively.

$$v_{impure}(\tau)/v_{pure} = \left[1 - 2\frac{a^2\kappa}{kT\sigma} n_{max}\theta_e(1 - e^{-\tau/\tau_i})^{1/2}\right]^{1/2} \quad \text{C. V.} - \text{Langmuir} \tag{7}$$

$$v_{impure}(\tau)/v_{pure} = \left[1 - \frac{4n_{max}\theta_e(1 - e^{-\tau/\tau_i})d_0^2}{\sigma^2}\right] \quad \text{van der Eerden} - \text{Langmuir} \tag{8}$$

which we evaluate numerically because $\tau$ and $\sigma$ are correlated. We confront eqs 7 and 8 with the experimentally obtained values for velocity reduction of steps emanating from a dislocation source in the presence of impurities plotted as a function of terrace exposure time. As can be observed in Figure 7b, these models fail to predict the experimentally observed dependence, especially at higher exposure times. A number of potential causes for this discrepancy can be put forward: (i) the most likely cause is that the adsorbed impurities interact and cluster together at higher surface concentrations.[13] This would explain the behavior at longer time scales: the mean spacing between clustered impurity patches will be significantly larger than if the impurities are distributed at random. As such, the critical point in the C.V.-model where the mean impurity spacing becomes equal to the critical radius and complete growth cessation is reached is not achieved in this system. (ii) Seikagaku solutions contain multiple impurities (here we assume only one), which may compete for the same surface binding sites. (iii) During these experiments, supersaturation was changed by means of temperature (19−25 °C), which could affect the impurity surface concentration. Compensating for this effect would require detailed knowledge on $k_D$. Further elucidation of the operating impurity mechanism is however beyond the scope of this Article. Although the models do not properly reproduce the experimental data, an order of estimate of $\tau_i$ can be made by identifying the terrace time at which 50% reduction in step velocity is achieved, yielding ∼10 s.

Finally, it should be mentioned that the observations done during this work correspond well with etching experiments realized on terraces of spiral hillocks and 2D islands by Ono and co-workers.[30] They found that many shallow etch pits were formed on terraces of 2D islands but almost none on terraces of spiral hillocks. For tetragonal lysozyme, it has been demonstrated that point defects (shallow etch pits) are related to incorporated impurities in the crystal lattice.[31,32] Hence, these results suggest a larger impurity incorporation during 2D-mediated growth, which is a consequence of the larger amount of adsorbed impurity molecules on the terraces between 2D island steps.

**Causes of Step Bunching in Lysozyme Crystal Growth.** Figure 5 manifests that spiral hillocks on lysozyme crystals grown at constant supersaturation from purified solution show much less pronounced step bunching than spiral hillocks growing in the presence of impurities. Hence, it seems reasonable to assume that the formation of bunched steps is directly related to the interaction with impurities and not only to intrinsic kinetic instabilities, as has been previously reported for the model system lysozyme.[33,34]

Additionally, the evolution of spiral growth and step bunching during growth from highly purified and commercial grade solution (98.5%, Seikagaku) showed that a progressive development of step bunching occurs with respect to the distance steps travel relative to their origin, that is, spiral dislocation outcrop. Taking into account that during lysozyme growth from contaminated solutions impurity adsorption is time dependent, which is a crucial assumption in the mechanisms for impurity-induced step bunching proposed by van der Eerden and Muller-Krumbhaar,[35,36] these qualitative data presented here strongly indicate that impurities play a decisive role in the process of step bunching during spiral growth. The observation of step bunching during growth from highly purified solution (99.99%) can be explained considering our previous works where we reported impurity effects in the case of the 99.99% pure solution for 2D nucleation[15] and step advancement.[25] The relationship between supersaturation and step bunching is not completely clear, but from the experimental data obtained in this work it seems that with increasing supersaturation, step bunching was reduced. This seems reasonable when considering impurities as an important cause of step bunching. At higher supersaturations, the influence of impurities on the step advancement is reduced considerably, mainly because the exposure time of the terraces to the impurities is reduced, and thus less step bunching should be expected. Even so, more experimental data are necessary to confirm this and obtain a better understanding of the step bunching mechanism.

## ■ CONCLUDING REMARKS AND FUTURE PERSPECTIVES

Spiral and 2D nucleation-mediated growth, in the absence of impurities, on the {110} face of tetragonal lysozyme lead to linear growth rate dependencies on $C - C_e$. If crystals are grown from contaminated solutions and the characteristic absorption time of impurities overlaps with the terrace exposure times, spiral growth can lead to crystals of increased purity due to reduced impurity adsorption on the surface. Preliminary LCM-DIM testing combined with theoretical simulations on a second model system, glucose isomerase, seems to confirm that for relatively fast impurity adsorption kinetics such a discrepancy between spiral and 2D-mediated growth is not so apparent. To fully corroborate such a claim, supersaturation dependencies of both step morphology and step kinetics need to be determined. We note that Maruyama and co-workers[37] have witnessed experimentally that spiral growth from contaminated solution under forced flow also experiences less impurity effects. This indicates that the model presented in our work also applies to different growth environments and therefore is of general interest. Although Maruyama et al. and our observations are quite promising to explain why crystals grown at similar supersaturation can have such different


dx.doi.org/10.1021/cg300024f | Cryst. Growth Des. XXXX, XXX, XXX−XXX

diffraction properties (taking into account that protein crystals can grow with both mechanisms for similar conditions), the results presented here should not be considered as a golden rule: "Spiral growth will always lead to superior X-ray quality crystals." This is due to several factors: (1) different faces of a same crystal can grow by distinct mechanisms, which induces different levels of purity for different growth sectors leading to accumulation of stress inside of the crystals; and (2) step bunching during spiral growth is directly related to the presence of impurities in the growth solution, and it is generally accepted that bunched steps induce striation, which leads to poorer diffraction properties.

## AUTHOR INFORMATION


### Corresponding Author

*Phone: +34 958230000 ext190109. Fax: +34 958 55 26 20. E-mail: sander@lec.csic.es.


### Notes

The authors declare no competing financial interest.

## ACKNOWLEDGMENTS

We are grateful for the support by Grant No. AYA2009-10655 of the Ministry of Science and Innovation, Spain, and the Consolider-Ingenio 2010 project "Factoría Española de crystalización" (A.E.S.V.D.). M.S. is grateful for the support by ESA/Prodex under contract number ESA AO-2004-070. This work has been carried out as a part of Project Research B in the Center for Interdisciplinary Research, Tohoku University, as well as "Ground-based Research Announcement for Space Utilization" promoted by the Japan Space Forum.

## REFERENCES


(1) Bott, R. R.; Navia, M. A.; Smith, J. L. *J. Biol. Chem.* **1982**, *257*, 9883−9886.

(2) Caylor, C. L.; Dobrianov, I.; Lemay, S. G.; Kimmer, C.; Kriminski, S.; Finkelstein, K. D.; Zipfel, W.; Webb, W. W.; Thomas, B. R.; Chernov, A. A.; Thorne, R. E. *Proteins* **1999**, *36*, 270−281 , DA-19990902.

(3) Yoshizaki, I.; Fukuyama, S.; Koizumi, H.; Tachibana, M.; Kojima, K.; Matsuura, Y.; Tanaka, M.; Igarashi, N.; Kadowaki, A.; Rong, L.; Adachi, S.; Yoda, S.; Komatsu, H. *J. Cryst. Growth* **2006**, *290*, 185−191.

(4) Yoshizaki, I.; Kadowaki, A.; Iimura, Y.; Igarashi, N.; Yoda, S.; Komatsu, H. *J. Synchrotron Radiat.* **2003**, *11*, 30−33.

(5) McPherson, A. *Crystallization of Biological Macromolecules*; Cold Spring Harbor Laboratory Press: New York, 1999.

(6) Vekilov, P. G.; Monaco, L. A.; Thomas, B. R.; Stojanoff, V.; Rosenberger, F. *Acta Crystallogr., Sect. D: Biol. Crystallogr.* **1996**, *52*, 785−798.

(7) Yau, S. T.; Thomas, B. R.; Vekilov, P. G. *J. Cryst. Growth* **2001**, *232*, 188−194.

(8) Malkin, A. J.; Kuznetsov, Y. G.; Land, T. A.; De Yoreo, J. J. *Nat. Struct. Biol.* **1995**, *2*, 956−959.

(9) McPherson, A.; Malkin, A. J.; Kuznetsov, Y. G.; Plomp, M. *Acta Crystallogr., Sect. D: Biol. Crystallogr.* **2001**, *57*, 1053−1060.

(10) McPherson, A.; Kuznetsov, Y. G.; Malkin, A.; Plomp, M. *J. Struct. Biol.* **2003**, *142*, 32−46 , DA-20030429.

(11) Vekilov, P. G.; Rosenberger, F. *J. Cryst. Growth* **1996**, *158*, 540−551.

(12) Heijna, M. C. R.; van Wamel, F. F. M.; van Enckevort, W. J. P.; Vlieg, E. *Cryst. Growth Des.* **2008**, *7*, 1999−2008.

(13) Nakada, T.; Sazaki, G.; Miyashita, S.; Durbin, S. D.; Komatsu, H. *J. Cryst. Growth* **1999**, *196*, 503−510.

(14) Feeling-Taylor, A. R.; Yau, S. T.; Petsev, D. N.; Nagel, R. L.; Hirsch, R. E.; Vekilov, P. G. *Biophys. J.* **2004**, *87*, 2621−2629 , DA-20040929.

(15) Van Driessche, A. E. S.; Sazaki, G.; Otalora, F.; Gonzalez-Rico, F. M.; Dold, P.; Tsukamoto, K.; Nakajima, K. *Cryst. Growth Des.* **2007**, *7*, 1980−1987.

(16) Sleutel, M.; Willaert, R.; Gillespie, C.; Evrard, C.; Wyns, L.; Maes, D. *Cryst. Growth Des.* **2008**, *9*, 497−504.

(17) Sleutel, M.; Maes, D.; Van Driessche, A. E. S. *Adv. Chem. Phys.* **2012**, *151*, 223−276.

(18) Sazaki, G.; Matsui, T.; Tsukamoto, K.; Usami, N.; Ujihara, T.; Fujiwara, K.; Nakajima, K. *J. Cryst. Growth* **2004**, *262*, 536−542.

(19) Van Driessche, A. E. S.; Otalora, F.; Sazaki, G.; Sleutel, M.; Tsukamoto, K.; Gavira, J. A. *Cryst. Growth Des.* **2008**, *8*, 4316−4323.

(20) Van Driessche, A. E. S.; Otalora, F.; Gavira, J. A.; Sazaki, G. *Cryst. Growth Des.* **2008**, *8*, 3623−3629.

(21) Sazaki, G.; Tsukamoto, K.; Yai, S.; Okada, M.; Nakajima, K. *Cryst. Growth Des.* **2005**, *5*, 1729−1735.

(22) Thomas, B. R.; Vekilov, P. G.; Rosenberger, F. *Acta Crystallogr., Sect. D: Biol. Crystallogr.* **1996**, *52*, 776−784.

(23) Sophianopoulos, A. J.; Rhodes, C. K.; Holcomb, D. N.; Van Holde, K. E. *J. Biol. Chem.* **1962**, *237*, 1107−1112.

(24) Durbin, S.; Feher, G. *J. Mol. Biol.* **1990**, *212*, 763−774.

(25) Van Driessche, A. E. S.; Sazaki, G.; Dai, G.; Otalora, F.; Gavira, J. A.; Matsui, T.; Yoshizaki, I.; Tsukamoto, K.; Nakajima, K. *Cryst. Growth Des.* **2009**, *9*, 3062−3071.

(26) Markov, I. V. *Crystal Growth for Beginners: Fundamentals of Nucleation, Crystal Growth and Epitaxy*; World Scientific Publishing: Singapore, 2003.

(27) Weaver, M. L.; Qiu, S. R.; Friddle, R. W.; Casey, W. H.; De Yoreo, J. J. *Cryst. Growth Des.* **2010**, *10*, 2954−2959.

(28) van der Eerden, J. P. In *Handbook of Crystal Growth*; Hurle, D. T. J., Ed.; North-Holland: Amsterdam, 1994; Vol. *1a*, pp 307−476.

(29) Friddle, R. W.; Weaver, M. L.; Qiu, S. R.; Wierzbicki, A.; Casey, W. H.; De Yoreo, J. J. *Proc. Natl. Acad. Sci. U.S.A.* **2010**, *107*, 11−15.

(30) Ono, E.; Dold, P.; Koizumi, K.; Tsukamoto, K.; Sazaki, G. International School on Biological Crystallization Granada, Spain, May 22−26, 2006.

(31) Hondoh, H.; Nakada, T. *Jpn. J. Appl. Phys.* **2004**, *43*, 4529−4532.

(32) Hondoh, H.; Nakada, T. *J. Cryst. Growth* **2005**, *275*, e1423−e1429.

(33) Vekilov, P. G.; Alexander, J. I.; Rosenberger, F. *Phys. Rev. E* **1996**, *54*, 6650−6660 , DA-19990210.

(34) Vekilov, P. G.; Rosenberger, F.; Lin, H.; Thomas, B. R. *J. Cryst. Growth* **1999**, *196*, 261−275.

(35) van der Eerden, J. P.; Muller-Krumbhaar, H. *Phys. Rev. Lett.* **1986**, *57*, 2431−2433.

(36) van der Eerden, J. P.; Müller-Krumbhaar, H. *Electrochim. Acta* **1986**, *31*, 1007−1012.

(37) Maruyama, M.; Kawahara, H.; Sazaki, G.; Maki, S.; Takahashi, Y.; Yoshikawa, H.; Sugiyama, S.; Adachi, H.; Takano, K.; Matsumura, H.; Inoue, T.; Murakami, S.; Mori, Y. *Cryst. Growth Des.*, submitted.